

THE LIPSCHITZ MATRIX: A TOOL FOR PARAMETER SPACE DIMENSION REDUCTION*

JEFFREY M. HOKANSON[†] AND PAUL G. CONSTANTINE[†]

Abstract. Assuming a multivariate function is Lipschitz continuous is one way to arrive at the curse of dimensionality—the situation where the cost of tasks such as approximation, integration, and optimization grow exponentially in the input dimension of the function. Here we introduce the Lipschitz matrix, a generalization of the scalar Lipschitz constant that alters the norm in which the distance between points is measured. When this Lipschitz matrix is low-rank, we are able to avoid this curse by noting that the quantity of interest is a ridge function with a low-dimensional subspace (the range of the Lipschitz matrix) onto which we can restrict the input without loss. Even if the Lipschitz matrix is not low rank, it can still reduce the constant associated with these tasks compared the Lipschitz constant when the singular values of the Lipschitz matrix decay. In addition, the Lipschitz matrix has other uses: it can identify an active subspace for parameter space dimension reduction; it can define uncertainty and provide informative bounds in high-dimensional spaces; and it motivates a space filling design of experiments to minimize uncertainty. As there are a limited number of situations where the Lipschitz matrix can be identified analytically, we show that the Lipschitz matrix can be estimated by solving a semidefinite program using a finite number of function samples or gradients.

Key words. Lipschitz matrix, subspace-based dimension reduction, design of computer experiments, uncertainty quantification, ridge function, information based complexity

AMS subject classifications. 26B35, 62K05, 68Q25

DOI.

1. Introduction. With the increasing sophistication of computer models, practitioners in science and engineering are often confronted with the *curse of dimensionality*: the phenomena that for many tasks, the computational burden grows exponentially in the number of parameters [26]. A common approach to confront this difficulty is to employ *dimension reduction* to identify a few parameters that are sufficient to (approximately) explain the behavior of the model. One important class of dimension reduction approaches are *subspace-based dimension reduction* techniques that identify a low-dimensional *active subspace* of the input parameters that approximately captures the variation in the function; e.g., given the function $f : \mathcal{D} \subset \mathbb{R}^m \rightarrow \mathbb{R}$ the active subspace spanned by the columns of $\mathbf{U} \in \mathbb{R}^{m \times n}$ allows f to be approximated by a *ridge function* of fewer parameters:

$$(1.1) \quad f(\mathbf{x}) \approx g(\mathbf{U}^\top \mathbf{x}); \quad g : \mathbb{R}^n \rightarrow \mathbb{R}, \quad \mathbf{U}^\top \mathbf{U} = \mathbf{I}.$$

There are a variety of approaches to identify this active subspace; see, e.g., the average outer-product of gradients [6] and ridge approximation [7, 13]. Here we introduce a new approach for parameter space dimension reduction based on a generalization of the scalar Lipschitz constant. This *Lipschitz matrix* not only allows us to identify the active subspace, but also provides improvements over the scalar Lipschitz constant: tightening the bounds on the uncertainty in the function away from samples and reducing the complexity of approximation, optimization, and integration.

*Submitted to the editors 31 May 2019.

Funding: This work is supported by DARPA’s program Enabling Quantification of Uncertainty in Physical Systems (EQUIPS).

[†] Department of Computer Science, University of Colorado Boulder, 1111 Engineering Dr, Boulder, CO 80309, (Jeffrey.Hokanson@colorado.edu, Paul.Constantine@colorado.edu).

Given a positive scalar Lipschitz constant $L \in \mathbb{R}_+$, we can define the class of Lipschitz functions on a domain $\mathcal{D} \subset \mathbb{R}^m$ with respect to the 2-norm

$$(1.2) \quad \mathcal{L}(\mathcal{D}, L) := \{f : \mathcal{D} \rightarrow \mathbb{R} : |f(\mathbf{x}_1) - f(\mathbf{x}_2)| \leq L \|\mathbf{x}_1 - \mathbf{x}_2\|_2, \forall \mathbf{x}_1, \mathbf{x}_2 \in \mathcal{D}\}.$$

To obtain the *Lipschitz matrix*, we move the scalar Lipschitz constant L inside the norm, promoting it to a matrix $\mathbf{L} \in \mathbb{R}^{m \times m}$. This yields an analogous class of Lipschitz functions with the Lipschitz matrix \mathbf{L} :

$$(1.3) \quad \mathcal{L}(\mathcal{D}, \mathbf{L}) := \{f : \mathcal{D} \rightarrow \mathbb{R} : |f(\mathbf{x}_1) - f(\mathbf{x}_2)| \leq \|\mathbf{L}(\mathbf{x}_1 - \mathbf{x}_2)\|_2, \forall \mathbf{x}_1, \mathbf{x}_2 \in \mathcal{D}\}.$$

We refer to both of these classes as *Lipschitz functions* as with the appropriate choice of scalar Lipschitz constant and Lipschitz matrix these two classes are nested:

$$(1.4) \quad \mathcal{L}(\mathcal{D}, \mathbf{L}) \subset \mathcal{L}(\mathcal{D}, \|\mathbf{L}\|_2) \quad \text{and} \quad \mathcal{L}(\mathcal{D}, L) = \mathcal{L}(\mathcal{D}, \mathbf{L}\mathbf{I}).$$

The advantage of the Lipschitz matrix over the Lipschitz constant is it provides additional information about the function. As an example of how this information can be exploited, consider a one-dimensional ridge function f_1 with scalar Lipschitz constant L_1 and Lipschitz matrix \mathbf{L}_1 :

$$(1.5) \quad f_1 : \mathcal{D}_1 = [-1, 1]^m \rightarrow \mathbb{R}, \quad f_1(\mathbf{x}) := g_1(\mathbf{a}^\top \mathbf{x}), \quad g_1 \in \mathcal{L}(\mathbb{R}, 1), \quad L_1 = \|\mathbf{a}\|_2, \quad \mathbf{L}_1 = \begin{bmatrix} \mathbf{0} \\ \mathbf{a}^\top \end{bmatrix}.$$

Suppose we seek approximate f_1 with error at most ϵ over \mathcal{D}_1 . Treating f_1 as a scalar Lipschitz function $f_1 \in \mathcal{L}(\mathcal{D}_1, L_1)$ would require us to sample at $\mathcal{O}(\epsilon^{-m})$ points in \mathcal{D} to minimize the worst-case error (see, e.g., [8, sec. 7])—this exponentially increasing cost with dimension m is the *curse of dimensionality*. However if we knew f_1 had Lipschitz matrix \mathbf{L}_1 , i.e., $f_1 \in \mathcal{L}(\mathcal{D}_1, \mathbf{L}_1)$, we could exploit the rank-1 nature of \mathbf{L}_1 and achieve the same worst case accuracy using only $\mathcal{O}(\epsilon^{-1})$ samples. Even if the Lipschitz matrix is not low rank, it can reduce the costs associated approximation as discussed in section 6.

One challenge when working with the Lipschitz matrix compared to the Lipschitz constant is there is no unique smallest Lipschitz matrix. For the scalar Lipschitz constant, the smallest Lipschitz constant is given by

$$(1.6) \quad \begin{aligned} & \underset{L \in \mathbb{R}_+}{\text{minimize}} \quad L \\ & \text{such that } |f(\mathbf{x}_1) - f(\mathbf{x}_2)| \leq L \|\mathbf{x}_1 - \mathbf{x}_2\|_2 \quad \forall \mathbf{x}_1, \mathbf{x}_2 \in \mathcal{D}. \end{aligned}$$

To pose an analogous optimization problem for the Lipschitz matrix, a total ordering of matrices $\mathbf{L} \in \mathbb{R}^{m \times m}$ must be provided. A partial ordering is provided by the symmetric positive semidefinite *squared Lipschitz matrix* $\mathbf{H} := \mathbf{L}^\top \mathbf{L}$ appearing in the constraint for Lipschitz matrix functions (1.3)

$$(1.7) \quad \|\mathbf{L}(\mathbf{x}_1 - \mathbf{x}_2)\|_2^2 = (\mathbf{x}_1 - \mathbf{x}_2)^\top \mathbf{L}^\top \mathbf{L} (\mathbf{x}_1 - \mathbf{x}_2) = (\mathbf{x}_1 - \mathbf{x}_2)^\top \mathbf{H} (\mathbf{x}_1 - \mathbf{x}_2).$$

Here we choose to introduce a total ordering compatible with this partial ordering of \mathbf{H} via the Frobenius norm and define the Lipschitz matrix \mathbf{L} to be the solution of

$$(1.8) \quad \begin{aligned} & \underset{\mathbf{L} \in \mathbb{R}^{m \times m}}{\text{minimize}} \quad \|\mathbf{L}\|_F^2 \\ & \text{such that } |f(\mathbf{x}_1) - f(\mathbf{x}_2)| \leq \|\mathbf{L}(\mathbf{x}_1 - \mathbf{x}_2)\|_2 \quad \forall \mathbf{x}_1, \mathbf{x}_2 \in \mathcal{D}. \end{aligned}$$

In many cases we will not be able to solve this problem exactly, but instead will approximate its solution given a finite number of evaluations of f and its gradient ∇f . In section 2, we show that the finite-data analog to (1.8) can be solved as semidefinite program in \mathbf{H} .

Unfortunately many functions that appear in computational science and engineering which are ideally Lipschitz functions, are not in practice due to *computational noise* [19]—a phenomena emerging due to many factors, including convergence tolerances and mesh discretizations. If we model the numerical function f as the sum of a true function \widehat{f} and a small perturbation \widetilde{f} , see, e.g., [19, eq. (1.3)],

$$(1.9) \quad f(\mathbf{x}) = \widehat{f}(\mathbf{x}) + \widetilde{f}(\mathbf{x})$$

we can extend our notion of Lipschitz to functions like f provided we can bound the perturbation from noise $\widetilde{f}(\mathbf{x})$. If $|\widetilde{f}(\mathbf{x})| \leq \frac{\epsilon}{2}$ for all $\mathbf{x} \in \mathcal{D}$, then f is an ϵ -Lipschitz function, where

$$(1.10) \quad f \in \mathcal{L}_\epsilon(\mathcal{D}, \mathbf{L}) := \{f(\mathbf{x}) + \eta : f \in \mathcal{L}(\mathcal{D}, \mathbf{L}), \eta \in [-\epsilon/2, \epsilon/2]\}.$$

In subsection 2.2 we show how to extend our estimation of the Lipschitz matrix from data to the ϵ -Lipschitz case.

Equipped with the Lipschitz matrix for a function f , we can use the knowledge that $f \in \mathcal{L}(\mathcal{D}, \mathbf{L})$ to aid in several applications. One way is to use the Lipschitz matrix to estimate the active subspace for a subspace-based dimension reduction. Analogously to the average outer product of gradients approach advocated by Constantine [6], choosing the active subspace of f to be the dominant eigenvectors of squared Lipschitz matrix \mathbf{H} minimizes an error bound in Theorem 3.1. Note that in terms of gradients, the squared Lipschitz matrix is an upper bound on the gradients in the ordering of positive semidefinite matrices, whereas the average outer product of gradients \mathbf{C} is a mean with respect to a measure ρ :

$$(1.11) \quad \mathbf{C} := \int_{\mathcal{D}} \nabla f(\mathbf{x}) \nabla f(\mathbf{x})^\top \rho(\mathbf{x}) \, d\mathbf{x} \quad \text{versus} \quad \nabla f(\mathbf{x}) \nabla f(\mathbf{x})^\top \preceq \mathbf{L}^\top \mathbf{L} = \mathbf{H} \quad \forall \mathbf{x} \in \mathcal{D},$$

where $\mathbf{A} \preceq \mathbf{B}$ denotes $\mathbf{B} - \mathbf{A}$ is positive semidefinite. As illustrated in section 3 the Lipschitz matrix yields similar active subspaces to the average outer product of gradients and has the advantage of not requiring gradient information. Additionally, the ϵ -Lipschitz matrix can avoid identifying an undesirable active subspace in the presence of high-frequency, low amplitude terms in f .

The Lipschitz matrix can also be used to define *uncertainty*—the range of possible values f might take away from its value known at samples. Unlike the uncertainty associated with the scalar Lipschitz constant, the Lipschitz matrix can provide informative uncertainty intervals as shown in section 4. This uncertainty estimate then motivates a space-filling *design of experiments* to minimize the Lipschitz matrix uncertainty. As illustrated in section 5, using this sampling scheme further reduces the uncertainty given the same number of samples.

As a final application of the Lipschitz matrix, we consider the worst case *information based complexity* of approximation, integration, and optimization for Lipschitz-matrix functions. In section 6 we show that the complexity of these tasks is proportional to the determinant of the Lipschitz matrix. As such, when the Lipschitz matrix has decaying singular values the computational cost can be substantially reduced compared to results using the Lipschitz constant. Moreover, when the Lipschitz matrix

is rank- r then f is an r -dimensional ridge function $f(\mathbf{x}) = g(\mathbf{U}^\top \mathbf{x})$ with $\mathbf{U} \in \mathbb{R}^{m \times r}$ and computational complexity scales with r instead of the intrinsic dimension of \mathcal{D} .

Following the principles of reproducible research, we provide code implementing the algorithms described in this paper and scripts generating the data appearing in the figures and tables available at <http://github.com/jeffrey-hokanson/PSDR/>.

2. Estimating the Lipschitz Matrix From Data. Ideally, given a function f we could identify its Lipschitz matrix analytically. Unfortunately, for many functions this is impractical. Instead we seek to estimate the Lipschitz matrix using a finite number of observations of the functions value $f(\hat{\mathbf{x}}_j)$ and its gradient $\nabla f(\check{\mathbf{x}}_j)$. In this section we show that the finite data analogue to (1.8) can be solved using a semidefinite program for both Lipschitz and ϵ -Lipschitz functions. We then discuss the possibility of low-rank solutions and using the determinant rather than the Frobenius norm to impose an ordering on Lipschitz matrices. Finally, we provide a numerical example illustrating the computational cost associated with finding the Lipschitz matrix and the convergence of these finite-data Lipschitz matrix estimates.

2.1. Semidefinite Program. After limiting our knowledge of f to a finite number of samples $\{f(\hat{\mathbf{x}}_j)\}_{j=1}^M$, the optimization problem for \mathbf{L} (1.8) becomes

$$(2.1) \quad \begin{aligned} & \underset{\mathbf{L} \in \mathbb{R}^{m \times m}}{\text{minimize}} \quad \|\mathbf{L}\|_{\text{F}}^2 \\ & \text{such that} \quad |f(\hat{\mathbf{x}}_i) - f(\hat{\mathbf{x}}_j)|^2 \leq \|\mathbf{L}(\hat{\mathbf{x}}_i - \hat{\mathbf{x}}_j)\|_2^2 \quad \forall i, j \in \{1, \dots, M\} \end{aligned}$$

By squaring the constraint, we note this is a non-convex quadratically constrained quadratic program. If instead we work with the squared Lipschitz matrix $\mathbf{H} := \mathbf{L}^\top \mathbf{L}$, we can identify the Lipschitz matrix by solving a convex program. Working over the cone of positive semidefinite matrices $\mathbb{S}_+^m \subset \mathbb{R}^{m \times m}$ and noting $\|\mathbf{L}\|_{\text{F}}^2 = \text{Tr } \mathbf{H}$, we solve

$$(2.2) \quad \begin{aligned} & \underset{\mathbf{H} \in \mathbb{S}_+^m}{\text{minimize}} \quad \text{Tr } \mathbf{H} \\ & \text{such that} \quad |f(\hat{\mathbf{x}}_i) - f(\hat{\mathbf{x}}_j)|^2 \leq (\hat{\mathbf{x}}_i - \hat{\mathbf{x}}_j)^\top \mathbf{H} (\mathbf{x}_i - \mathbf{x}_j) \quad \forall i, j \in \{1, \dots, M\} \end{aligned}$$

and recover \mathbf{L} as the unique symmetric positive semidefinite square root of \mathbf{H} .

If gradient information is available, we can include this data to estimate the Lipschitz matrix. Recalling the Lipschitz constraint in (1.8) for points $\mathbf{x} \in \mathcal{D}$ and $\mathbf{x} + \delta \mathbf{p} \in \mathcal{D}$ where $\mathbf{p} \in \mathbb{R}^m$, the Lipschitz matrix \mathbf{L} , and thus \mathbf{H} , must satisfy

$$(2.3) \quad |f(\mathbf{x} + \delta \mathbf{p}) - f(\mathbf{x})|^2 \leq \|\mathbf{L}(\mathbf{x} + \delta \mathbf{p} - \mathbf{x})\|_2^2 = \delta^2 \mathbf{p}^\top \mathbf{L}^\top \mathbf{L} \mathbf{p} = \delta^2 \mathbf{p}^\top \mathbf{H} \mathbf{p}.$$

Then dividing by δ^2 and taking the limit as $\delta \rightarrow 0$, we have

$$(2.4) \quad (\mathbf{p}^\top \nabla f(\mathbf{x}))^2 = \mathbf{p}^\top \nabla f(\mathbf{x}) \nabla f(\mathbf{x})^\top \mathbf{p} \leq \mathbf{p}^\top \mathbf{H} \mathbf{p}.$$

Since this must hold for any $\mathbf{p} \in \mathbb{R}^m$, we conclude

$$(2.5) \quad \nabla f(\mathbf{x}) \nabla f(\mathbf{x})^\top \preceq \mathbf{H}.$$

Thus, incorporating the gradient at $\{\check{\mathbf{x}}_j\}_{j=1}^N$ yields the semidefinite program:

$$(2.6) \quad \begin{aligned} & \underset{\mathbf{H} \in \mathbb{S}_+^m}{\text{minimize}} \quad \text{Tr } \mathbf{H} \\ & \text{such that} \quad |f(\hat{\mathbf{x}}_i) - f(\hat{\mathbf{x}}_j)|^2 \leq (\hat{\mathbf{x}}_i - \hat{\mathbf{x}}_j)^\top \mathbf{H} (\hat{\mathbf{x}}_i - \hat{\mathbf{x}}_j) \quad \forall 1 \leq i < j \leq M, \\ & \quad \quad \quad \nabla f(\check{\mathbf{x}}_k) \nabla f(\check{\mathbf{x}}_k)^\top \preceq \mathbf{H} \quad \forall k = 1, \dots, N. \end{aligned}$$

In our numerical examples, we use CVXOPT [1] to solve (2.2) and (2.6).

Note that the Lipschitz class of functions (1.3) does not constrain second and higher derivatives; hence these derivatives cannot be added to (2.6) to constrain the Lipschitz matrix.

2.2. ϵ -Lipschitz. We follow a similar approach to identify the ϵ -Lipschitz matrix associated with a function f . From the definition of this function class in (1.10), we note that for any two points $\mathbf{x}_1, \mathbf{x}_2 \in \mathcal{D}$, f must satisfy

$$(2.7) \quad |f(\mathbf{x}_1) - f(\mathbf{x}_2)| \leq \epsilon + \|\mathbf{L}(\mathbf{x}_1 - \mathbf{x}_2)\|_2.$$

Then given samples $\{\hat{\mathbf{x}}_j\}_{j=1}^M$ we find the squared Lipschitz matrix \mathbf{H} as the solution of a semidefinite program

$$(2.8) \quad \begin{aligned} & \text{minimize } \text{Tr } \mathbf{H} \\ & \mathbf{H} \in \mathbb{S}_+^m \\ & \text{such that } (|f(\hat{\mathbf{x}}_i) - f(\hat{\mathbf{x}}_j)| - \epsilon)^2 \leq (\hat{\mathbf{x}}_i - \hat{\mathbf{x}}_j)^\top \mathbf{H} (\hat{\mathbf{x}}_i - \hat{\mathbf{x}}_j) \quad \forall 1 \leq i < j \leq M. \end{aligned}$$

Note that due to the inclusion of ϵ in (2.7), the class of ϵ -Lipschitz functions does not constrain derivatives. Hence we cannot use derivative information in (2.8) unlike the standard Lipschitz case (2.6).

2.3. Low Rank Solutions. It is tempting to impose a rank constraint on \mathbf{H} to yield low-rank Lipschitz matrices satisfying the data. Unfortunately this can yield uninformative estimates of low-rank structure. For example, given only samples of f at points $\{\hat{\mathbf{x}}_j\}_{j=1}^M$ in general position, almost every vector $\mathbf{a} \in \mathbb{R}^m$ yield distinct projections $\{\mathbf{a}^\top \hat{\mathbf{x}}_j\}_{j=1}^M$ and hence we can find a rank-1 Lipschitz matrix:

$$(2.9) \quad \mathbf{L} = \begin{bmatrix} \mathbf{0} \\ \alpha \mathbf{a}^\top \end{bmatrix} \in \mathbb{R}^{m \times m}, \quad \alpha = \max_{i,j} \frac{|f(\hat{\mathbf{x}}_i) - f(\hat{\mathbf{x}}_j)|}{|\mathbf{a}^\top \hat{\mathbf{x}}_i - \mathbf{a}^\top \hat{\mathbf{x}}_j|}.$$

Gradient information improves this situation; if $\text{Span}\{\nabla f(\check{\mathbf{x}}_j)\}_{j=1}^N$ is an r -dimensional subspace of \mathbb{R}^m , then \mathbf{H} and \mathbf{L} must be at least rank r .

2.4. Using the Determinant. Later, in section 6 we show the computational complexity of several tasks is proportional to the determinant of the Lipschitz matrix. So, we might ask: why not use $\det \mathbf{L}$ in the optimization for the Lipschitz matrix (2.6)? There are two important reasons. First, we lose convexity: $\|\mathbf{L}\|_{\text{F}}^2 = \text{Tr } \mathbf{H}$ is convex whereas $|\det \mathbf{L}|^2 = \det \mathbf{H}$ is concave. Second, as illustrated in the previous subsection, given only finite samples we can always find a low-rank Lipschitz matrix; hence minimizing the determinant would always terminate with a zero objective value but a likely spurious solution.

Even though we are not minimizing the determinant, minimizing the Frobenius norm minimizes a bound on the determinant. Using Jensen's inequality,

$$(2.10) \quad |\det \mathbf{L}|^2 = \det \mathbf{H} \leq m^{-m} \text{Tr}(\mathbf{H})^m = m^{-m} \|\mathbf{L}\|_{\text{F}}^{2m}.$$

2.5. Convergence. Figure 2.1 provides a numerical example illustrating the convergence of Lipschitz matrix estimates with increasing data using the six dimensional OTL Circuit test function [4]. Here we have used the Frobenius norm to measure the convergence of \mathbf{H} to a 'true' estimate $\hat{\mathbf{H}}$ based on a large number of gradient samples. As an alternative to the Frobenius norm, we could have used the

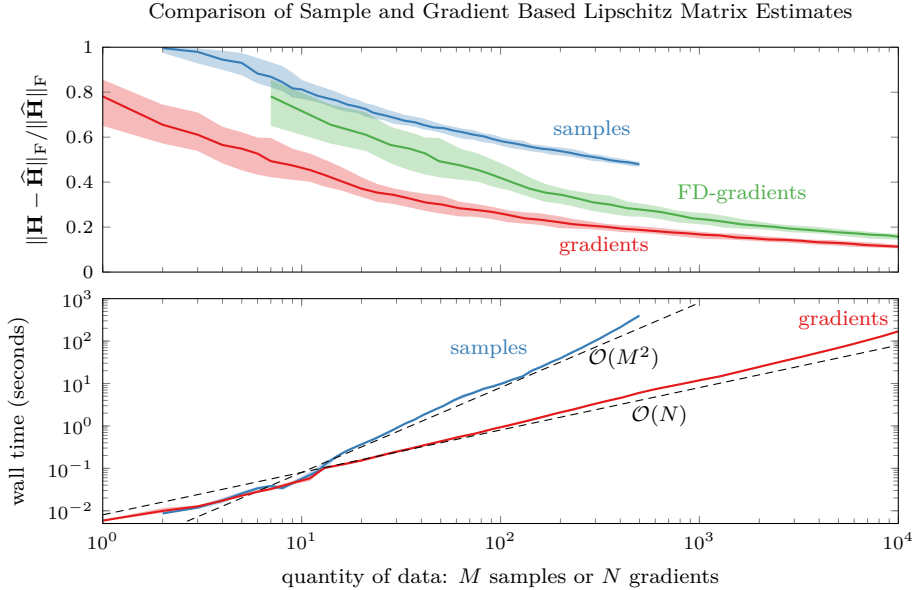


FIG. 2.1. The convergence of an estimate of the squared Lipschitz matrix using either samples or gradients. Here we estimate the ‘true’ Lipschitz matrix $\hat{\mathbf{H}}$ using 6^6 gradient samples on an evenly spaced tensor product grid. The Lipschitz matrix \mathbf{H} is estimated using samples drawn uniformly at random from the domain. As the number of function and gradient samples increases, the top plot shows that the estimate \mathbf{H} converges to the nominal value $\hat{\mathbf{H}}$. The bottom plot shows the wall-clock time taken to solve the linear or semidefinite program using CVXOPT on a Xeon E5-2620 clocked at 2.1 GHz using OpenBLAS. For each plot the median is shown as a solid line the shaded region encloses the 25th to 75th percentile estimated from 100 repetitions.

geodesic distance on the space of positive definite matrices [5, eq. (2.5)]:

$$(2.11) \quad d_{\mathbb{S}_+^m}(\mathbf{H}_1, \mathbf{H}_2) = \sqrt{\sum_k \log^2(\lambda_k(\mathbf{H}_1, \mathbf{H}_2))}$$

where $\lambda_k(\mathbf{H}_1, \mathbf{H}_2)$ denotes the k th generalized eigenvalue of the pencil $\lambda\mathbf{H}_1 - \mathbf{H}_2$. However in this example the Lipschitz matrix was low-rank when using a small number of samples and hence the distance was undefined.

Two features are immediately apparent in this example. As expected, as the quantity of data increases our estimates of the squared Lipschitz matrix converge to their nominal value. Further, we note that the computation time scales roughly linear in the number of gradients, but quadratic in the number of samples. Both cases result from growth in the number of constraints imposed. Given the slower convergence of the sample-based estimate of the Lipschitz matrix and its greater computational expense, we might ask: is it better to construct finite-difference based gradients than use the samples directly? In this example with random samples, the answer is yes. However this only works because we our evaluations of f are noise-free and hence we are able to accurately compute derivatives from finite-differences.

Finally we note that computing the Lipschitz matrix is far more computationally expensive than a Monte Carlo estimate of the average outer product of gradients \mathbf{C} (1.11) using the same number of gradients; here constructing \mathbf{C} always took less than 10^{-2} seconds even with $N = 10^4$ gradient samples.

3. Dimension Reduction. Broadly speaking, parameter space dimension reduction consists of finding a low-dimensional set of coordinates resulting from a map \mathbf{h} where

$$(3.1) \quad f(\mathbf{x}) \approx g(\mathbf{h}(\mathbf{x})), \quad g: \mathbb{R}^n \rightarrow \mathbb{R}, \quad \mathbf{h}: \mathcal{D} \rightarrow \mathbb{R}^n,$$

Broadly speaking, there are three main classes of parameter space dimension reduction distinguished by their class of \mathbf{h} . *Coordinate-based* dimension reduction identifies a set of active parameters denoted by the index set \mathcal{I} along which f varies and chooses \mathbf{h} to select these parameters

$$(3.2) \quad [\mathbf{h}(\mathbf{x})]_i = [\mathbf{x}]_{\mathcal{I}[i]}.$$

There are a variety of ways to identify these active variables; see, e.g., [27] for a review. *Subspace-based* dimension reduction identifies an *active subspace* spanned by the columns of $\mathbf{U} \in \mathbb{R}^{m \times n}$ along which f varies and chooses \mathbf{h} to be a linear function

$$(3.3) \quad \mathbf{h}(\mathbf{x}) = \mathbf{U}^\top \mathbf{x}.$$

As with coordinate-based approaches, there are a variety of methods for identifying the active subspace such as the average outer product of gradients [6], polynomial ridge approximation [13], and many others [17]. *Nonlinear* dimension reduction permits \mathbf{h} to be any nonlinear function and includes a variety of approaches; see, e.g., [16]. Note these classes are nested: coordinate-based approaches are a subset of subspace-based approaches where \mathbf{U} is restricted to be columns of the identity matrix; subspace-based approaches are a subset of nonlinear approaches where \mathbf{h} is restricted to be linear.

In this section we show that the Lipschitz matrix can be used to identify an active subspace via the dominant eigenvectors of the squared Lipschitz matrix. Much like the average outer product of gradients, we can motivate our choice of subspace via an approximation error bound given in Theorem 3.1 involving the eigenvalues of \mathbf{H} . We show in subsection 3.2 that rapid decay of eigenvalues indicates low-dimensional structure and show in subsection 3.3 that projecting onto the dominant eigenvectors of \mathbf{H} yields similar subspaces to existing methods when applied to a common test problem. However there are examples where existing approaches identify an active subspace that is not useful. Although the standard Lipschitz approach fails in a similar way, we show that ϵ -Lipschitz can avoid this pitfall in subsection 3.4.

3.1. Error Bound. When using the Lipschitz matrix in the context of subspace-based dimension reduction, our goal will be to find a ridge approximation \tilde{f} of f where

$$(3.4) \quad f(\mathbf{x}) \approx \tilde{f}(\mathbf{x}) := g(\mathbf{U}^\top \mathbf{x}), \quad \mathbf{U}^\top \mathbf{U} = \mathbf{I},$$

where g is called the *ridge profile*. Note that for vectors \mathbf{w} in the nullspace of \mathbf{U} , the ridge function \tilde{f} has the same value for \mathbf{x} and $\mathbf{x} + \mathbf{w}$:

$$(3.5) \quad |\tilde{f}(\mathbf{x} + \mathbf{w}) - \tilde{f}(\mathbf{x})| = |g(\mathbf{U}^\top (\mathbf{x} + \mathbf{w})) - g(\mathbf{U}^\top \mathbf{x})| = |g(\mathbf{U}^\top \mathbf{x}) - g(\mathbf{U}^\top \mathbf{x})| = 0.$$

Hence the Lipschitz matrix of \tilde{f} has the same nullspace as \mathbf{U} . Thus when seeking a ridge approximation of the Lipschitz function $f \in \mathcal{L}(\mathcal{D}, \mathbf{L})$ with an active subspace spanned by the columns of \mathbf{U} , we will construct our approximation from $\mathcal{L}(\mathcal{D}, \mathbf{L}\mathbf{U}\mathbf{U}^\top)$. The following theorem provides a bound on the accuracy of a ridge approximation.

THEOREM 3.1. *Suppose $f \in \mathcal{L}(\mathcal{D}, \mathbf{L})$ and $\tilde{f} \in \mathcal{L}(\mathcal{D}, \mathbf{L}\mathbf{U}\mathbf{U}^\top)$ where $\mathbf{U} \in \mathbb{R}^{m \times n}$ and $\mathbf{U}^\top \mathbf{U} = \mathbf{I}$. If $|f(\hat{\mathbf{x}}_j) - \tilde{f}(\hat{\mathbf{x}}_j)| \leq \epsilon$ and $\max_{\mathbf{x} \in \mathcal{D}} \min_j \|\mathbf{L}\mathbf{U}\mathbf{U}^\top(\hat{\mathbf{x}}_j - \mathbf{x})\|_2 \leq \delta$ then*

$$(3.6) \quad \max_{\mathbf{x} \in \mathcal{D}} |f(\mathbf{x}) - \tilde{f}(\mathbf{x})| \leq \epsilon + 2\delta + \sigma_{\max}(\mathbf{L}(\mathbf{I} - \mathbf{U}\mathbf{U}^\top)) \cdot \text{diam}(\mathcal{D})$$

where $\sigma_{\max}(\mathbf{A})$ denotes the largest singular value of \mathbf{A} and $\text{diam}(\mathcal{D})$ denotes the diameter of the set \mathcal{D} .

Proof. Suppose $\mathbf{x} \in \mathcal{D}$ is fixed and let $j = \text{argmin}_k \|\mathbf{L}\mathbf{U}\mathbf{U}^\top(\hat{\mathbf{x}}_k - \mathbf{x})\|_2$. Then as $|f(\hat{\mathbf{x}}_j) - \tilde{f}(\hat{\mathbf{x}}_j)| \leq \epsilon$ we have

$$(3.7) \quad |f(\mathbf{x}) - \tilde{f}(\mathbf{x})| = |f(\mathbf{x}) - \tilde{f}(\mathbf{x}) + [f(\hat{\mathbf{x}}_j) - \tilde{f}(\hat{\mathbf{x}}_j)] - [f(\hat{\mathbf{x}}_j) - \tilde{f}(\hat{\mathbf{x}}_j)]|$$

$$(3.8) \quad \leq |f(\mathbf{x}) - f(\hat{\mathbf{x}}_j)| + |\tilde{f}(\mathbf{x}) - \tilde{f}(\hat{\mathbf{x}}_j)| + \epsilon.$$

After invoking each function's Lipschitz matrix

$$(3.9) \quad \leq \|\mathbf{L}(\mathbf{x} - \hat{\mathbf{x}}_j)\|_2 + \|\mathbf{L}\mathbf{U}\mathbf{U}^\top(\mathbf{x} - \hat{\mathbf{x}}_j)\|_2 + \epsilon$$

$$(3.10) \quad \leq \|\mathbf{L}(\mathbf{U}\mathbf{U}^\top + \mathbf{I} - \mathbf{U}\mathbf{U}^\top)(\mathbf{x} - \hat{\mathbf{x}}_j)\|_2 + \|\mathbf{L}(\mathbf{U}\mathbf{U}^\top)(\mathbf{x} - \hat{\mathbf{x}}_j)\|_2 + \epsilon,$$

and using the triangle inequality in the first term,

$$(3.11) \quad \leq 2\|\mathbf{L}(\mathbf{U}\mathbf{U}^\top)(\mathbf{x} - \hat{\mathbf{x}}_j)\|_2 + \|\mathbf{L}(\mathbf{I} - \mathbf{U}\mathbf{U}^\top)(\mathbf{x} - \hat{\mathbf{x}}_j)\|_2 + \epsilon$$

$$(3.12) \quad \leq \epsilon + 2\delta + \sigma_{\max}(\mathbf{L}(\mathbf{I} - \mathbf{U}\mathbf{U}^\top)) \cdot \text{diam}(\mathcal{D}). \quad \square$$

Hence by choosing \mathbf{U} to be the right singular vectors of \mathbf{L} associated with the largest singular values, we can minimize this bound. If we slightly rewrite this result in terms of the eigenvalues of the squared Lipschitz matrix,

$$(3.13) \quad \sigma_{\max}(\mathbf{L}(\mathbf{I} - \mathbf{U}\mathbf{U}^\top))^2 = \lambda_{\max}((\mathbf{I} - \mathbf{U}\mathbf{U}^\top)\mathbf{H}(\mathbf{I} - \mathbf{U}\mathbf{U}^\top)),$$

we can make a connection to the error bound associated with the average outer product of gradients.

THEOREM 3.2 (Constantine [6, Thm 4.3]). *If $\mathcal{D} \subset \mathbb{R}^m$ is convex with Poincaré constant C , $\rho : \mathcal{D} \rightarrow \mathbb{R}_+$ is a probability density function with $\rho(\mathbf{x}) \leq R \forall \mathbf{x} \in \mathcal{D}$, and $\mathbf{C} := \int_{\mathbf{x} \in \mathcal{D}} \nabla f(\mathbf{x}) \nabla f(\mathbf{x})^\top d\rho(\mathbf{x})$, then the optimal ridge approximation onto the subspace spanned by \mathbf{U} is given by*

$$(3.14) \quad g(\mathbf{y}) = \int f(\mathbf{U}\mathbf{y} + \mathbf{W}\mathbf{z}) \pi_{Z|Y}(\mathbf{z}) d\mathbf{z}, \quad \text{with} \quad \begin{bmatrix} \mathbf{U} & \mathbf{W} \end{bmatrix}^\top \begin{bmatrix} \mathbf{U} & \mathbf{W} \end{bmatrix} = \mathbf{I}$$

with an associated error bound

$$(3.15) \quad \int (f(\mathbf{x}) - g(\mathbf{U}^\top \mathbf{x}))^2 d\rho(\mathbf{x}) \leq (RC)^2 \cdot \text{Tr}((\mathbf{I} - \mathbf{U}\mathbf{U}^\top)\mathbf{C}(\mathbf{I} - \mathbf{U}\mathbf{U}^\top)).$$

3.2. Eigenvalue Decay. When using the average outer product of gradients, the presence of low-dimensional structure is assessed by noting a strong decay in the eigenvalues of \mathbf{C} ; the same argument can be made for the squared Lipschitz matrix \mathbf{H} . Table 3.1 show the eigenvalues of both matrices estimated using random gradient samples corresponding to a Monte-Carlo estimate of \mathbf{C} . Three features are revealed in this example. First is that the eigenvalues of the squared Lipschitz matrix are always greater than those of the average outer product of gradients; this is unsurprising as

TABLE 3.1

Eigenvalues of the average outer product of gradients \mathbf{C} and squared Lipschitz matrix \mathbf{H} on three test problems estimated using 1000 gradient samples selected randomly from the domain with uniform probability.

i	OTL Circuit [4]		Borehole [12]		Wing Weight [10]	
	$\lambda_i(\mathbf{C})$	$\lambda_i(\mathbf{H})$	$\lambda_i(\mathbf{C})$	$\lambda_i(\mathbf{H})$	$\lambda_i(\mathbf{C})$	$\lambda_i(\mathbf{H})$
1	$4.5 \cdot 10^0$	$1.4 \cdot 10^1$	$6.6 \cdot 10^3$	$3.6 \cdot 10^4$	$7.1 \cdot 10^3$	$1.9 \cdot 10^4$
2	$1.7 \cdot 10^{-1}$	$2.2 \cdot 10^0$	$5.3 \cdot 10^1$	$3.0 \cdot 10^3$	$1.2 \cdot 10^2$	$3.4 \cdot 10^3$
3	$4.6 \cdot 10^{-2}$	$1.2 \cdot 10^0$	$8.6 \cdot 10^0$	$6.4 \cdot 10^2$	$5.7 \cdot 10^1$	$1.3 \cdot 10^3$
4	$8.6 \cdot 10^{-3}$	$3.4 \cdot 10^{-1}$	$2.0 \cdot 10^0$	$3.8 \cdot 10^2$	$1.8 \cdot 10^1$	$7.8 \cdot 10^2$
5	$1.2 \cdot 10^{-4}$	$2.8 \cdot 10^{-2}$	$8.6 \cdot 10^{-1}$	$8.0 \cdot 10^1$	$1.7 \cdot 10^1$	$5.9 \cdot 10^2$
6	$6.8 \cdot 10^{-9}$	$2.5 \cdot 10^{-4}$	$9.5 \cdot 10^{-3}$	$1.3 \cdot 10^1$	$6.6 \cdot 10^0$	$3.8 \cdot 10^2$
7			$9.4 \cdot 10^{-9}$	$3.3 \cdot 10^{-3}$	$5.9 \cdot 10^{-1}$	$9.0 \cdot 10^1$
8			$3.0 \cdot 10^{-16}$	$2.0 \cdot 10^{-5}$	$6.8 \cdot 10^{-2}$	$2.2 \cdot 10^1$
9					$1.2 \cdot 10^{-2}$	$5.4 \cdot 10^0$
10					$2.3 \cdot 10^{-4}$	$6.5 \cdot 10^{-1}$

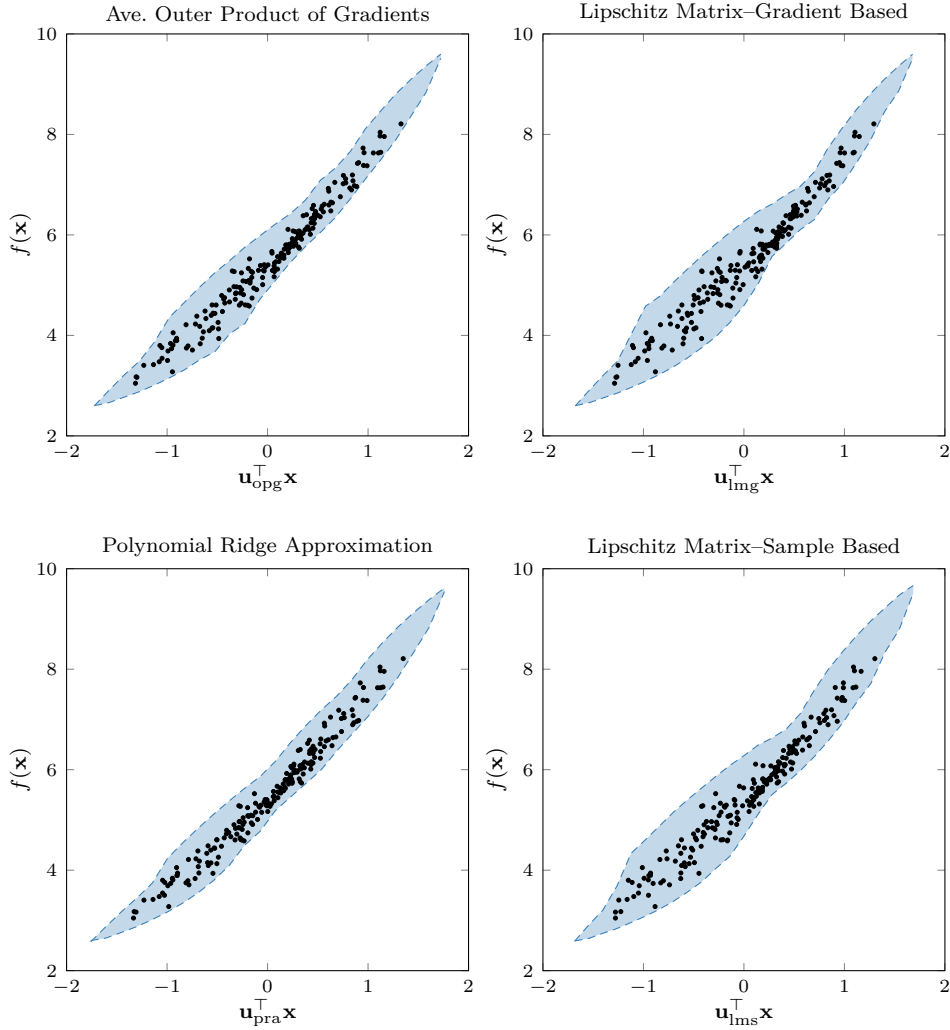
\mathbf{H} is an upper bound on the outer product of gradients $\nabla f(\mathbf{x})\nabla f(\mathbf{x})^\top$ whereas \mathbf{C} is an average; cf. (1.11). Second, the decay of eigenvalues for \mathbf{H} is slower than that of \mathbf{C} for the same reason. Third, we note that it is harder to identify low-rank Lipschitz matrices than low-rank structure in the average outer product of gradients. The borehole test function is a seven-dimensional ridge function and, as such, both \mathbf{C} and \mathbf{H} should be rank-7. This is clearly evident the eigenvalues of \mathbf{C} , but less so in the eigenvalues of \mathbf{H} due to the increased difficulty of solving the semidefinite program for \mathbf{H} along with the associated solver tolerances (although there still is a nine order of magnitude decrease in the eigenvalues of \mathbf{H}).

3.3. Shadow Plots. One advantage of subspace-based dimension reduction is the ability to visualize high-dimensional functions via shadow plots. These plots, illustrated in Figure 3.1 for one-dimensional approximations, show the projection of the input \mathbf{x} onto a one-dimensional subspace defined by $\mathbf{u} \in \mathbb{R}^m$ along the horizontal axis and the value of the function along the vertical axis, collapsing the $m - 1$ orthogonal dimensions into the page. This example shows three different methods for computing the active subspace: the Lipschitz matrix, the average outer-product of gradients [6], and a polynomial ridge approximation [13]. Given either function samples or gradient samples, each method yields a similar estimate of the active subspace.

3.4. ϵ -Lipschitz. Although the dominant eigenvectors of the squared Lipschitz matrix often identify a good subspace, this approach can be fooled by highly oscillatory but small amplitude components of a function. As an example, consider the “corrugated roof” function [7, eq. (26)]:

$$(3.16) \quad f : [-1, 1]^2 \rightarrow \mathbb{R}, \quad f(\mathbf{x}) = 5x_1 + \sin(10\pi x_2).$$

In this case we can compute the Lipschitz matrix analytically: $\mathbf{H} = \begin{bmatrix} 25 & 0 \\ 0 & 100\pi^2 \end{bmatrix}$. Taking as the active subspace the span of the dominant eigenvector $[0, 1]^\top$ yields projection that is not useful for predicting the value of f as shown in Figure 3.2. This direction was identified because the although the contribution of the sine term is small, its gradients are large. The ϵ -Lipschitz approach offers away around this. Choosing $\epsilon = 2$ the contribution of the sine term is ignored, leaving the rank-1 squared Lipschitz matrix $\mathbf{H}_2 = \begin{bmatrix} 25 & 0 \\ 0 & 0 \end{bmatrix}$. Then taking the active subspace to be the span of dominant



Method	R_{b_1}	R_{b_2}	R_f	R_{c_1}	R_{c_2}	β
Ave. Outer Product of Gradients	-0.75	0.61	0.24	-0.13	-0.0002	-0.0034
Lipschitz Matrix-Gradient	-0.79	0.58	0.19	-0.13	-0.0001	-0.0012
Polynomial Ridge Approximation	-0.71	0.64	0.26	-0.13	-0.0079	-0.0062
Lipschitz Matrix-Sample	-0.77	0.61	0.17	-0.11	0.0065	-0.0262

FIG. 3.1. An illustration of the active subspaces identified by different subspace-based dimension reduction methods on the OTL circuit function on the normalized domain $\mathcal{D} = [-1, 1]^6$. The table below shows the weight vector associated with the best one-dimensional subspace identified by each method. The first two methods use 200 gradient samples to estimate this subspace, whereas the second two methods use 200 function samples. The plot above shows the one-dimensional shadow plot—the projection of the six-dimensional input onto a single linear combination. Dots show the 200 samples used to generate this reduction and the shaded region is an estimate the projection of function f onto this one-dimensional subspace. Note that each of these four plots projects onto a different subspace, which we emphasize by using a different label on the horizontal axis in each plot.

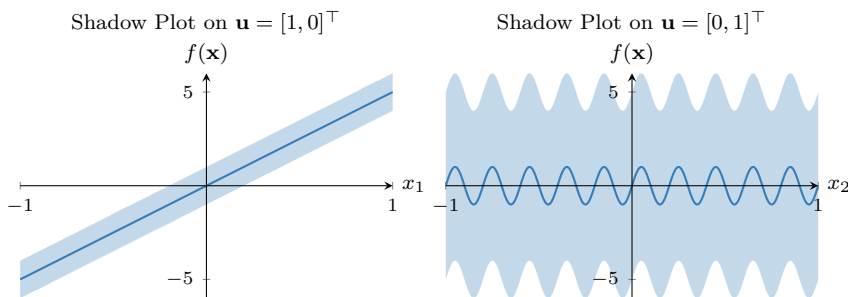


FIG. 3.2. Two shadow plots of the corrugated roof function (3.16). The solid line denotes the mean value, the shaded area denotes the area of possible oscillation.

eigenvector of this matrix $[1, 0]^\top$ yields a substantially more predictive projection as seen in Figure 3.2. Although this is a toy example, this illustrates how the ϵ -Lipschitz matrix can avoid being influenced by spurious computational noise which the sine term emulates.

4. Uncertainty. When working with expensive deterministic computer simulations it is often necessary to employ an approximation of certain quantities of interest, called a *response surface* or a *surrogate*. Supposing we have constructed this approximation using samples of f , it is natural ask: what are the range of possible values our approximation could take away from these samples? This is often called *uncertainty* in this setting. Gaussian processes provide one approach to define an uncertainty [21, sec. 2.2]; the Lipschitz constant provides another [22]. Here we show that scalar Lipschitz uncertainty can be generalized to the Lipschitz matrix setting, and that the Lipschitz matrix provides a much tighter estimate of uncertainty than the corresponding scalar Lipschitz constant.

Before continuing, it is important to note that the Gaussian process and Lipschitz notions of uncertainty are based on very different assumptions. The Gaussian process perspective views the approximation f as a random process with prior

$$(4.1) \quad \tilde{f} \sim \mathcal{GP}(m(\mathbf{x}), k(\mathbf{x}, \mathbf{x}'))$$

where $m : \mathcal{D} \rightarrow \mathbb{R}$ is the mean and $k : \mathcal{D} \times \mathcal{D} \rightarrow \mathbb{R}$ is a symmetric covariance kernel; see, e.g., [21, eq. (2.14)]. Information about f , the inputs $\hat{\mathbf{x}}_j$ and outputs $y_j := f(\hat{\mathbf{x}}_j)$, serve to condition this prior such that $\tilde{f}(\mathbf{x})$ is a normal random variable with mean and covariance given by [21, eq. (2.19)]:

$$(4.2) \quad \tilde{f}(\mathbf{x}) \sim \mathcal{N} \left(\begin{bmatrix} k(\mathbf{x}, \hat{\mathbf{x}}_1) \\ \vdots \\ k(\mathbf{x}, \hat{\mathbf{x}}_M) \end{bmatrix}^\top \begin{bmatrix} k(\hat{\mathbf{x}}_1, \hat{\mathbf{x}}_1) & \cdots & k(\hat{\mathbf{x}}_M, \hat{\mathbf{x}}_1) \\ \vdots & & \vdots \\ k(\hat{\mathbf{x}}_1, \hat{\mathbf{x}}_M) & \cdots & k(\hat{\mathbf{x}}_M, \hat{\mathbf{x}}_M) \end{bmatrix}^{-1} \begin{bmatrix} y_1 - m(\hat{\mathbf{x}}_1) \\ \vdots \\ y_M - m(\hat{\mathbf{x}}_M) \end{bmatrix}, \right. \\ \left. k(\mathbf{x}, \mathbf{x}) - \begin{bmatrix} k(\mathbf{x}, \hat{\mathbf{x}}_1) \\ \vdots \\ k(\mathbf{x}, \hat{\mathbf{x}}_M) \end{bmatrix}^\top \begin{bmatrix} k(\hat{\mathbf{x}}_1, \hat{\mathbf{x}}_1) & \cdots & k(\hat{\mathbf{x}}_M, \hat{\mathbf{x}}_1) \\ \vdots & & \vdots \\ k(\hat{\mathbf{x}}_1, \hat{\mathbf{x}}_M) & \cdots & k(\hat{\mathbf{x}}_M, \hat{\mathbf{x}}_M) \end{bmatrix}^{-1} \begin{bmatrix} k(\mathbf{x}, \hat{\mathbf{x}}_1) \\ \vdots \\ k(\mathbf{x}, \hat{\mathbf{x}}_M) \end{bmatrix} \right).$$

Uncertainty in the approximation \tilde{f} for a given probability threshold $\delta \in (0, 1)$ is then defined as all those values of $\tilde{f}(\mathbf{x})$ with probability greater than δ ; this is illustrated in Figure 4.1.

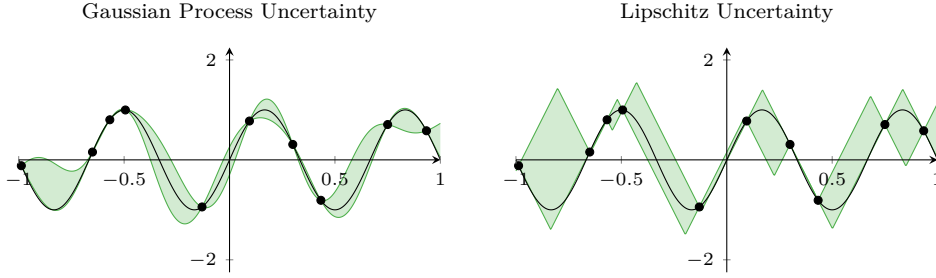


FIG. 4.1. A comparison of Gaussian Process and the Lipschitz notions of uncertainty. Here we use ten samples of $f(x) = \sin(3\pi x)$ on $\mathcal{D} = [-1, 1]$ denoted by dots, with f shown by the black line. In both plots, the shaded area denotes the uncertainty estimate. The left plot shows the Gaussian process with zero-mean $m(\mathbf{x}) = 0$ and squared exponential covariance $k(\mathbf{x}, \mathbf{x}') = \exp(-\frac{1}{2}\|\ell(\mathbf{x} - \mathbf{x}')\|_2^2)$ where $\ell = 0.157$ has been chosen to maximize the marginal likelihood [21, subsec. 2.7.1]; the probability threshold δ corresponds to one-standard deviation. The right plot shows the Lipschitz uncertainty with Lipschitz constant $L = 8.39$ estimated from the samples.

An alternative view of uncertainty posits f comes from some function class and that samples constrain the values f can take. Denoting this function class as \mathcal{F} , the set of values f could take at \mathbf{x} given $y_j := f(\hat{\mathbf{x}}_j)$ is the uncertainty set \mathcal{U} :

$$(4.3) \quad \mathcal{U}(\mathbf{x}; \mathcal{F}, \{(\hat{\mathbf{x}}_j, y_j)\}_{j=1}^M) := \{\tilde{f}(\mathbf{x}) : \tilde{f} \in \mathcal{F}, \tilde{f}(\hat{\mathbf{x}}_j) = y_j \forall j = 1, \dots, M\} \subset \mathbb{R}.$$

Here we choose the function class based on the Lipschitz matrix associated with f ; i.e., $\mathcal{F} = \mathcal{L}(\mathcal{D}, \mathbf{L})$. Figure 4.1 shows this uncertainty set is substantially different than the Gaussian process uncertainty.

In this section we provide a formula for the interval $\mathcal{U}(\mathbf{x})$ in subsection 4.1 and discuss how to project this interval onto a shadow plot in subsection 4.2. Combined with the Lipschitz-matrix based space filling design discussed in section 5 this allows us to provide informative bounds on shadow plots.

4.1. Uncertainty Interval. For Lipschitz functions $f \in \mathcal{L}(\mathcal{D}, \mathbf{L})$ the uncertainty set \mathcal{U} is an interval:

$$(4.4) \quad \mathcal{U}(\mathbf{x}; \mathcal{L}(\mathcal{D}, \mathbf{L}), \{(\hat{\mathbf{x}}_j, y_j)\}_{j=1}^M) = \{\tilde{y} : |\tilde{y} - y_j| \leq \|\mathbf{L}(\mathbf{x} - \hat{\mathbf{x}}_j)\|_2, \forall j = 1, \dots, M\}$$

$$(4.5) \quad = \left[\max_{j=1, \dots, M} y_j - \|\mathbf{L}(\mathbf{x} - \hat{\mathbf{x}}_j)\|_2, \min_{j=1, \dots, M} y_j + \|\mathbf{L}(\mathbf{x} - \hat{\mathbf{x}}_j)\|_2 \right].$$

Figure 4.2 shows the gap between the upper and lower limits of this interval when using both the scalar Lipschitz constant and the Lipschitz matrix; note the Lipschitz matrix yields far smaller uncertainty intervals.

4.2. Uncertainty on Shadow Plots. Given the utility of shadow plots in understanding the behaviour of high-dimensional functions, we seek to include a projection of uncertainty onto these plots. Each position α on the horizontal axis consists of all the points in \mathcal{D} where $\mathbf{u}^\top \mathbf{x} = \alpha$; i.e., the set $\mathcal{S}_\alpha := \{\mathbf{x} \in \mathcal{D} : \mathbf{u}^\top \mathbf{x} = \alpha\}$. Then the uncertainty associated with this position on the horizontal axis is the union of all the pointwise uncertainties in this set \mathcal{S}_α ; this motivates extending the definition of uncertainty for set valued inputs

$$(4.6) \quad \mathcal{U}(\mathcal{S}; \mathcal{F}, \{(\hat{\mathbf{x}}_j, y_j)\}_{j=1}^M) := \bigcup_{\mathbf{x} \in \mathcal{S}} \mathcal{U}(\mathbf{x}; \mathcal{F}, \{(\hat{\mathbf{x}}_j, y_j)\}_{j=1}^M).$$

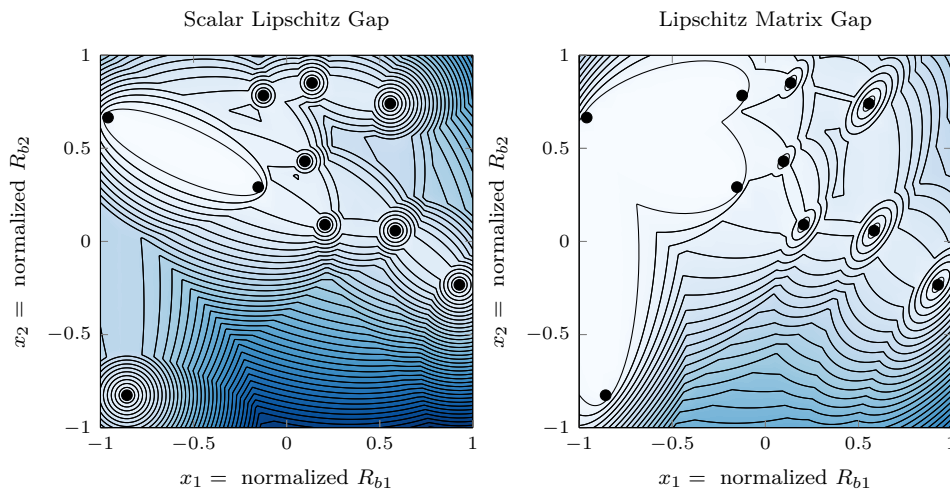


FIG. 4.2. A plot of the gap between the upper and lower Lipschitz bounds. Here we use function values taken the OTL circuit test problem using the first two parameters, holding the remainder at their central values; additionally the domain has been normalized to $[-1, 1]^2$. In each plot, the contours show an increase of 0.1 in the gap. Here the uncertainty set, the Lipschitz constant, and Lipschitz matrix were all estimated using the ten samples marked with dots. Here $L = 2.38$ and $\mathbf{L} = \begin{bmatrix} 1.6 & 0 \\ -1.3 & 1.6 \end{bmatrix}$.

For closed sets \mathcal{S} , the Lipschitz uncertainty is an interval whose boundaries are given by minimax optimization problems:

$$(4.7) \quad \mathcal{U}(\mathcal{S}; \mathcal{L}(\mathcal{D}, \mathbf{L}), \{(\hat{\mathbf{x}}_j, y_j)\}_{j=1}^M) = \left[\min_{\mathbf{x} \in \mathcal{S}} \max_{j=1, \dots, M} y_j - \|\mathbf{L}(\mathbf{x} - \hat{\mathbf{x}}_j)\|_2, \max_{\mathbf{x} \in \mathcal{S}} \min_{j=1, \dots, M} y_j + \|\mathbf{L}(\mathbf{x} - \hat{\mathbf{x}}_j)\|_2 \right].$$

Figure 4.3 shows an application of this set-based definition using both scalar and matrix Lipschitz on points placed at the corners of the domain and on points selected based on a space filling design as described in the next section. Unlike the estimate of the projection of the function in Figure 3.1, no new samples of f have been taken to construct the uncertainty in this figure.

Before concluding, briefly discuss solving the two minimax optimization problems in (4.7). Although there are sophisticated algorithms for problems of this type, we use a simple sequential linear program approach due to Osborne and Watson [20]. As these two optimization problems are similar, we only discuss the lower bound. Introducing a slack variable t to represent this lower bound, we seek to minimize

$$(4.8) \quad \underset{\mathbf{x} \in \mathcal{S}, t \in \mathbb{R}}{\text{minimize}} \quad t \quad \text{such that} \quad f(\hat{\mathbf{x}}_j) - \|\mathbf{L}(\mathbf{x} - \hat{\mathbf{x}}_j)\|_2 \leq t, \quad \forall j = 1, \dots, M.$$

Linearizing the constraints yields a sequence of linear programs for the update \mathbf{p} such that $\mathbf{x}^{(k+1)} = \mathbf{x}^{(k)} + \mathbf{p}$:

$$(4.9) \quad \underset{\mathbf{x}^{(k)} + \mathbf{p} \in \mathcal{S}, t \in \mathbb{R}}{\text{minimize}} \quad t \quad \text{such that} \quad f(\hat{\mathbf{x}}_j) - \|\mathbf{L}(\mathbf{x}^{(k)} - \hat{\mathbf{x}}_j)\|_2 - \frac{\mathbf{p}^\top \mathbf{L}^\top \mathbf{L}(\mathbf{x}^{(k)} - \hat{\mathbf{x}}_j)}{\|\mathbf{L}(\mathbf{x}^{(k)} - \hat{\mathbf{x}}_j)\|_2} \leq t, \quad \forall j.$$

As the 2-norm is convex and the search direction \mathbf{p} increases the norm, the Taylor series approximation provides a lower bound and each step of this iteration will be feasible, removing the need for a line search. One challenge in solving this optimization

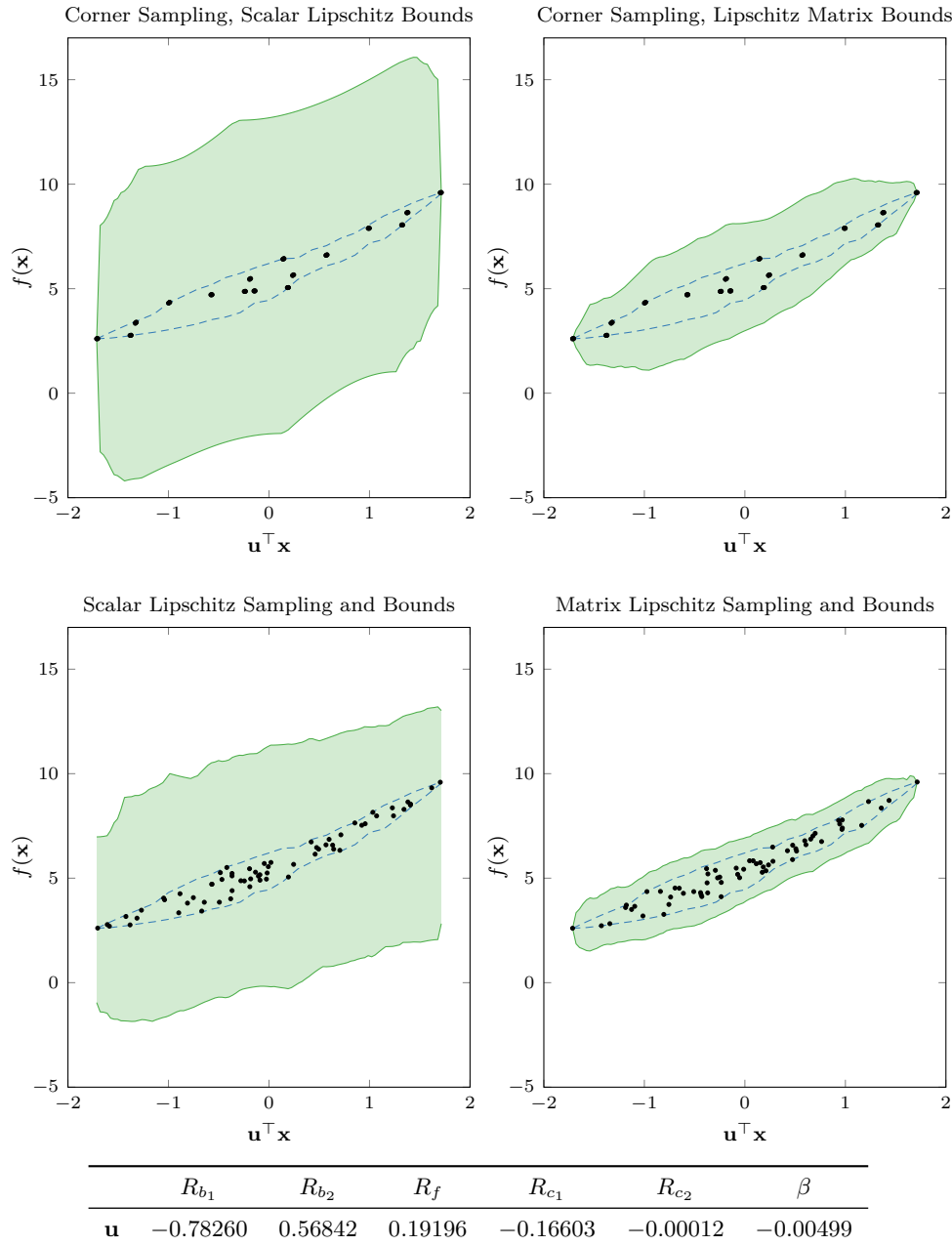


FIG. 4.3. Shadow plots of the OTL Circuit function on the normalized domain. Here we have projected onto the leading eigenvector \mathbf{u} shown above of the squared Lipschitz matrix \mathbf{H} estimated using gradients of f evaluated at the corners. The dots denote the value of the $2^6 = 64$ samples of f ; in the top two plots these samples are placed in the corners of the domain whereas in the bottom two plots these samples are placed using a sequential space-filling design discussed in section 5. The shaded region denotes the projected uncertainty interval (4.7) and the dashed region encloses the range of f based on 8^6 samples on a tensor-product grid. Due to the small values associated with trailing two entries in \mathbf{u} , the dots marking samples in the top row overlap.

problem is the large number of spurious local minimizers as evidenced in Figure 4.1. To ensure we obtain a nearly optimal objective value of (4.8) we try multiple initializations of the iteration (4.9) starting from random samples of the Voronoi vertices of $\{\widehat{\mathbf{x}}_j\}_{j=1}^M$ in the \mathbf{L} weighted 2-norm. These Voronoi vertices are discussed in more detail in the next section and play a central role there.

5. Design of Computer Experiments. Given the uncertainty derived from the Lipschitz matrix in the previous section, we might ask: how can we choose samples to minimize the size of the uncertainty interval (4.5)? This fundamentally is a question of the *design of computer experiments* [24], a subfield of the *design of experiments* (see, e.g., [9]) with the primary distinction that observations are deterministic; i.e., $f(\mathbf{x})$ returns only one value. Although there are a variety of motivations for constructing a design of experiments, here we show the Lipschitz matrix motivates a space-filling design of experiments in the metric induced by the Lipschitz matrix. We briefly describe how a design can be approximated using the vertices of the Voronoi diagram and discuss the pitfalls of a greedy, maximum uncertainty approach when the Lipschitz matrix is unknown.

5.1. Space Filling Design. In a space filling design (see, e.g., [23, sec. 5.3]) the goal is to distribute samples $\{\widehat{\mathbf{x}}_j\}_{j=1}^M$ evenly with respect to a particular distance metric on the domain of f . Here we use a metric derived from the Lipschitz matrix:

$$(5.1) \quad d(\mathbf{x}_1, \mathbf{x}_2) = \|\mathbf{L}(\mathbf{x}_1 - \mathbf{x}_2)\|_2.$$

For example, a *minimax distance design* would choose samples $\{\widehat{\mathbf{x}}_j\}_{j=1}^M$ to minimize the fill distance in this metric:

$$(5.2) \quad \underset{\widehat{\mathbf{x}}_1, \dots, \widehat{\mathbf{x}}_M \subset \mathcal{D}}{\text{minimize}} \max_{\mathbf{x} \in \mathcal{D}} \min_{j=1, \dots, M} \|\mathbf{L}(\widehat{\mathbf{x}}_j - \mathbf{x})\|_2.$$

We can motivate this design as it minimizes an error bound for all interpolatory approximations of f with the same Lipschitz matrix.

COROLLARY 5.1. *Suppose $f, \tilde{f} \in \mathcal{L}(\mathcal{D}, \mathbf{L})$ with $f(\widehat{\mathbf{x}}_j) = \tilde{f}(\widehat{\mathbf{x}}_j)$ for $j = 1, \dots, M$, then*

$$(5.3) \quad \max_{\mathbf{x} \in \mathcal{D}} |f(\mathbf{x}) - \tilde{f}(\mathbf{x})| \leq \max_{\mathbf{x} \in \mathcal{D}} \min_{j=1, \dots, M} 2\|\mathbf{L}(\widehat{\mathbf{x}}_j - \mathbf{x})\|_2.$$

Proof. Set $\mathbf{U} = \mathbf{I}$ and $\epsilon = 0$ in Theorem 3.1. □

Note, others have justified minimax designs using Bayesian arguments [14].

Unfortunately constructing a minimax design is challenging due to the nested optimization problem. Instead we solve a simpler optimization problem as a proxy for this minimax design that allows us to exploit tools from computational geometry to aid in its solution. Specifically we construct a sequential *maximin distance design* by picking $\widehat{\mathbf{x}}_{M+1}$ holding $\widehat{\mathbf{x}}_1, \dots, \widehat{\mathbf{x}}_M$ fixed:

$$(5.4) \quad \widehat{\mathbf{x}}_{M+1} = \underset{\mathbf{x} \in \mathcal{D}}{\text{argmax}} \min_{j=1, \dots, M} \|\mathbf{L}(\widehat{\mathbf{x}}_j - \mathbf{x})\|_2.$$

When \mathcal{D} is a convex polytope this is an example of the largest empty circle problem whose solution is given by the *bounded Voronoi vertices* [2, subsec. 5.1.3]. The Voronoi vertices are those points that are equidistant to their m closest points from $\{\mathbf{x}_j\}_{j=1}^M$:

$$(5.5) \quad \|\mathbf{L}(\mathbf{v} - \widehat{\mathbf{x}}_{\mathcal{I}[1]})\|_2 = \dots = \|\mathbf{L}(\mathbf{v} - \widehat{\mathbf{x}}_{\mathcal{I}[m]})\|_2 \leq \|\mathbf{L}(\mathbf{v} - \widehat{\mathbf{x}}_j)\|_2 \forall j = 1, \dots, M,$$

TABLE 5.1

Estimated maximum pointwise uncertainty over the domain using either Lipschitz constant or Lipschitz matrix based sequential maximin distance designs using one hundred samples. For comparison, each function's range has been normalized to $[0, 1]$.

test problem	dim.	Lipschitz constant max. uncertainty	Lipschitz matrix max. uncertainty	ratio
Golinski volume [11]	6	0.66	0.10	6.37
OTL circuit [4]	6	1.39	0.34	4.07
piston [15]	7	3.34	0.63	5.29
borehole [12]	8	3.60	0.47	7.70
wing weight [10]	10	1.89	0.39	4.88

and the bounded Voronoi vertices are those vertices inside \mathcal{D} along with the intersections of equidistance hyperplanes with the boundary of \mathcal{D} . If the domain \mathcal{D} is described by linear equality and inequality constraints $\mathcal{D} = \{\mathbf{x} \in \mathbb{R}^m : \mathbf{A}\mathbf{x} \leq \mathbf{b}, \mathbf{A}_{\text{eq}}\mathbf{x} = \mathbf{b}_{\text{eq}}\}$ then these bounded Voronoi vertices are those points that satisfy a total of m equality constraints:

$$(5.6) \quad \begin{aligned} \|\mathbf{L}(\mathbf{v} - \widehat{\mathbf{x}}_{\mathcal{I}(1)})\|_2 &= \dots = \|\mathbf{L}(\mathbf{v} - \widehat{\mathbf{x}}_{\mathcal{I}(\ell)})\|_2 \leq \|\mathbf{L}(\mathbf{v} - \widehat{\mathbf{x}}_j)\|_2 \quad \forall j = 1, \dots, M; \\ \mathbf{A}_{\text{eq}}\mathbf{v} &= \mathbf{b}_{\text{eq}} \quad \mathbf{A}_{\text{eq}} \in \mathbb{R}^{p \times m}, \mathbf{b}_{\text{eq}} \in \mathbb{R}^p; \\ \mathbf{A}_{\cdot, \mathcal{J}}\mathbf{v} &= \mathbf{b}_{\cdot, \mathcal{J}} \quad |\mathcal{J}| = m - \ell - p. \end{aligned}$$

By construction these bounded Voronoi vertices satisfy the KarushKuhnTucker conditions for (5.4) and hence are local minimizers of (5.4). Thus, one approach to solving (5.4) is to enumerate these bounded Voronoi vertices \mathbf{v} and simply return the vertex minimizing $\min_{j=1, \dots, M} \|\mathbf{L}(\widehat{\mathbf{x}}_j - \mathbf{v})\|_2$. In low dimensional spaces (i.e., $m = 3$) this is feasible using specialized solvers like Qhull [3]. However, the number of bounded Voronoi vertices grows exponentially in dimension of the domain and for higher dimensional spaces we resort to a randomized vertex sampling algorithm to find a subset of these [18].

5.2. Numerical Examples. Here we provide two examples to illustrate the effectiveness of using a Lipschitz matrix based design of experiments over one based on the Lipschitz constant. Table 5.1 shows an estimate of maximum pointwise uncertainty based on these two designs and shows that the maximum pointwise uncertainty is reduced by a factor of three to seven. In Figure 4.3 we see that the uncertainty projected onto the shadow plot is significantly reduced when using a Lipschitz matrix based design compared to a Lipschitz constant design. Importantly, the projected uncertainty is only a factor of two larger than the enclosing envelope based on hundreds of thousands of samples; this means the Lipschitz matrix coupled with a Lipschitz design of experiments can provide an informative projected uncertainty.

5.3. Maximum Uncertainty Design. A tempting heuristic for choosing samples sequentially is to pick the next sample $\widehat{\mathbf{x}}_{M+1}$ where the uncertainty interval (4.4) is largest; i.e.,

$$(5.7) \quad \widehat{\mathbf{x}}_{M+1} = \underset{\mathbf{x} \in \mathcal{D}}{\operatorname{argmax}} |\mathcal{U}(\mathbf{x}; \mathcal{L}(\mathcal{D}, \mathbf{L}), \{(\widehat{\mathbf{x}}_j, y_j)\}_{j=1}^M)|.$$

Unfortunately, this heuristic will fail if we are simultaneously trying to estimate the Lipschitz matrix from these samples. Namely, there can be regions of the domain

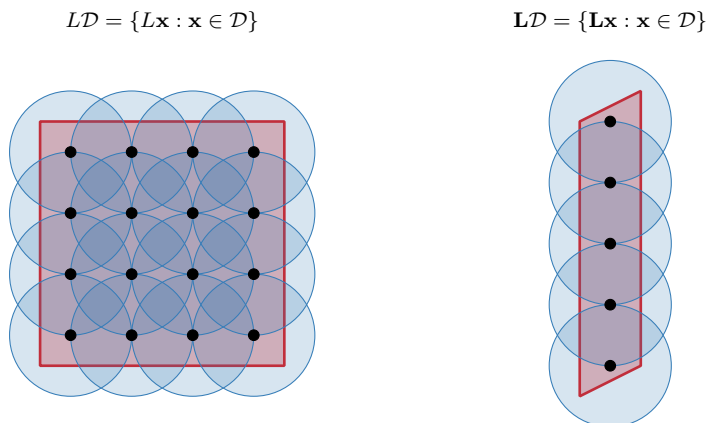


FIG. 6.1. A cartoon illustrating the interaction of the covering number with the Lipschitz matrix. Here we consider the domain $\mathcal{D} = [-1, 1]^2$ and a function with scalar Lipschitz constant $L = 4$ and a Lipschitz matrix $\mathbf{L} = \begin{bmatrix} 1 & 0 \\ -1 & 4 \end{bmatrix}$. The transformed domain is marked in red and the (suboptimal) covering centered at black dots with circles denoting the ϵ -balls. For the Lipschitz constant on the left, covering $L\mathcal{D}$ requires placing balls in both axes. For the Lipschitz matrix on the right covering $\mathbf{L}\mathcal{D}$ requires placing balls along only one axis. This illustrates how the Lipschitz matrix can slow the growth of the covering number in the pre-asymptotic regime. This example also shows how the Lipschitz matrix reduces the volume of the transformed domain; the volume of $\mathbf{L}\mathcal{D}$ is four times smaller than $L\mathcal{D}$.

where the Lipschitz bounds predict an uncertainty interval of size zero that also contain samples that would increase the Lipschitz matrix. This can be seen in one dimension in Figure 4.1. Near $\frac{1}{3}$ the bounds are tight, yet this region contains the maximum slope which, if sampled, would increase the Lipschitz constant.

6. Information Based Complexity. Whereas the last section sought samples minimizing uncertainty given a particular function, now we ask a related question: what is the minimum number of samples required approximate *any* $f \in \mathcal{L}(\mathcal{D}, \mathbf{L})$ to within ϵ throughout \mathcal{D} ? This is a question of *information based complexity* [26]: a subfield that seeks to understand the fundamental complexity of tasks such as approximation, integration, and optimization. For standard scalar Lipschitz functions $f \in \mathcal{L}(\mathcal{D}, L)$ these results are well known; see, e.g., [26, chap. 2]. In this section we generalize these complexity results for Lipschitz matrix functions. Our approach will be to connect the computational complexity to the ϵ *internal covering number* illustrated in Figure 6.1—given a domain \mathcal{D} , the number of ϵ balls centered at points $\hat{\mathbf{x}}_j \in \mathcal{D}$ covering the domain \mathcal{D} :

$$(6.1) \quad N_\epsilon(\mathcal{D}) := \operatorname{argmin}_{M, \{\hat{\mathbf{x}}_j\}_{j=1}^M \subset \mathcal{D}} M \text{ such that } \mathcal{D} \subseteq \bigcup_{j=1}^M \mathcal{B}_\epsilon(\hat{\mathbf{x}}_j), \quad \mathcal{B}_\epsilon(\hat{\mathbf{x}}_j) = \{\mathbf{x} : \|\mathbf{x} - \hat{\mathbf{x}}_j\|_2 \leq \epsilon\}.$$

Specifically, we will show that the worst-case computational complexity to obtain $\mathcal{O}(\epsilon)$ accuracy for approximation, integration, and optimization requires $N_\epsilon(\mathbf{L}\mathcal{D})$ evaluations of $f \in \mathcal{L}(\mathcal{D}, \mathbf{L})$ where $\mathbf{L}\mathcal{D} = \{\mathbf{L}\mathbf{x} : \mathbf{x} \in \mathcal{D}\}$.

The reason that the covering number plays a critical role in each of these tasks is that $N_\epsilon(\mathbf{L}\mathcal{D})$ is the minimum number of samples required to construct a minimax distance design (5.2) where every point in the domain is at most a distance ϵ away

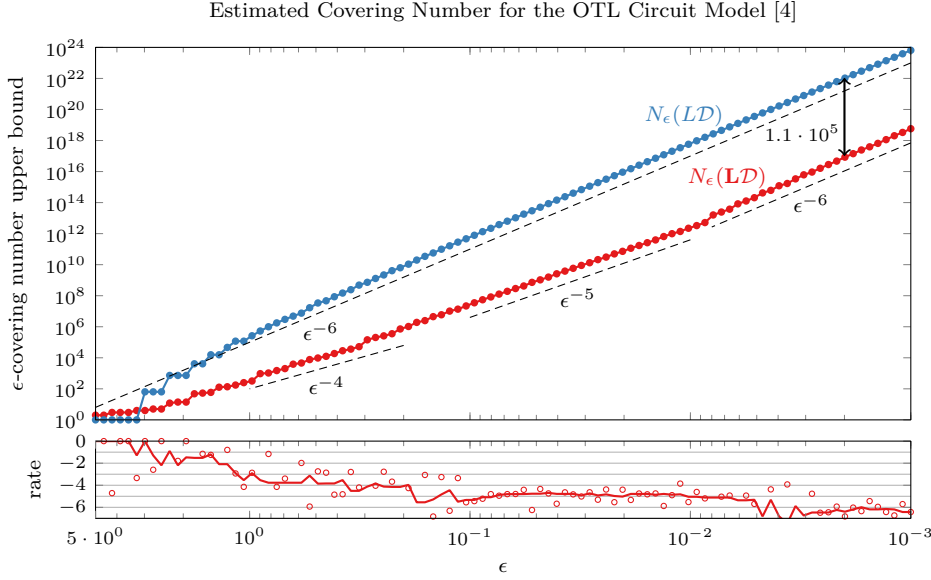


FIG. 6.2. An upper bound on the covering number of the transformed domain. Here we estimate the covering number by counting the number of ϵ -balls whose centers are on a grid with spacing $2\epsilon/\sqrt{m}$ that intersect the transformed domain; when the number of grid points exceeds 10^4 , random samples are used to estimate the number of ϵ -balls intersecting the domain. The bottom plot shows the estimated growth rate of $N_\epsilon(\mathbf{LD})$ estimated using a finite difference (dots) and a 7-point median smoothed rate (line). Note that the asymptotic separation of $1.1 \cdot 10^5$ matches the ratio $\text{vol}(\mathbf{LD})/\text{vol}(\mathbf{LD})$.

from a sample $\hat{\mathbf{x}}_j$. To see this, let $\hat{\mathbf{z}}_j$ be points in \mathbf{LD} forming an ϵ -covering:

$$(6.2) \quad \mathbf{LD} \subseteq \bigcup_{j=1}^{N_\epsilon(\mathbf{LD})} B_\epsilon(\hat{\mathbf{z}}_j), \quad \hat{\mathbf{z}} \in \mathbf{LD}.$$

Then we can then find points $\hat{\mathbf{x}}_j \in \mathcal{D}$ such that $\mathbf{L}\hat{\mathbf{x}}_j = \hat{\mathbf{z}}_j$ (these are non-unique if \mathbf{L} is low-rank). After changing coordinates the maximum distance is at most ϵ :

$$(6.3) \quad \max_{\mathbf{x} \in \mathcal{D}} \min_{j=1, \dots, N_\epsilon(\mathbf{LD})} \|\mathbf{L}(\mathbf{x} - \hat{\mathbf{x}}_j)\|_2 = \max_{\mathbf{z} \in \mathbf{LD}} \min_{j=1, \dots, N_\epsilon(\mathbf{LD})} \|\mathbf{z} - \hat{\mathbf{z}}_j\|_2 \leq \epsilon.$$

This connection to the covering number exposes a geometric origin for the curse of dimensionality. If $\mathcal{D} \subset \mathbb{R}^m$ is convex and contains at least one ϵ -ball then the covering number grows exponentially in the dimension m :

$$(6.4) \quad \left(\frac{1}{\epsilon}\right)^m \frac{\text{vol}(\mathcal{D})}{\text{vol}(\mathcal{B}_1)} \leq N_\epsilon(\mathcal{D}) \leq \left(\frac{3}{\epsilon}\right)^m \frac{\text{vol}(\mathcal{D})}{\text{vol}(\mathcal{B}_1)}.$$

where $\text{vol}(\mathcal{D})$ refers to the Lebesgue measure of the set in \mathbb{R}^m [28, Thm 14.2]. Note that if \mathcal{D} has an intrinsic dimension r less than m , then there an r -dimensional domain $\tilde{\mathcal{D}} \subset \mathbb{R}^r$ with intrinsic dimension r such that each point in $\tilde{\mathcal{D}}$ is associated with a unique point in \mathcal{D} . Hence to apply these bounds on the covering number (6.4) we must work on the transformed domain $\tilde{\mathcal{D}}$ rather than \mathcal{D} .

The bounds on the covering number in (6.4) suggest two ways that the Lipschitz matrix can reduce complexity that the scalar Lipschitz constant cannot. The more

TABLE 6.1

Comparison of Lipschitz matrix, Lipschitz constant, and corresponding volumes for a variety of test functions [25] posed on the normalized domain $\mathcal{D} = [-1, 1]^m$ with normalized outputs in $[0, 1]$. Here \mathbf{L} has been estimated using 1024 gradient samples including the 2^m corners and otherwise sampled randomly.

test problem	dim.	L	$\sigma_{\max}(\mathbf{L})$	$\sigma_{\min}(\mathbf{L})$	$\text{vol}(LD)$	$\text{vol}(\mathbf{LD})$
Golinski volume [11]	6	$3.0 \cdot 10^{-1}$	$3.0 \cdot 10^{-1}$	$7.3 \cdot 10^{-4}$	$4.3 \cdot 10^{-2}$	$8.4 \cdot 10^{-9}$
OTL circuit [4]	6	$5.4 \cdot 10^{-1}$	$5.8 \cdot 10^{-1}$	$1.4 \cdot 10^{-3}$	$1.6 \cdot 10^0$	$1.4 \cdot 10^{-5}$
piston [15]	7	$1.0 \cdot 10^0$	$1.0 \cdot 10^0$	$2.6 \cdot 10^{-3}$	$1.3 \cdot 10^2$	$2.0 \cdot 10^{-6}$
borehole [12]	8	$9.0 \cdot 10^{-1}$	$9.2 \cdot 10^{-1}$	$4.6 \cdot 10^{-6}$	$1.1 \cdot 10^2$	$5.0 \cdot 10^{-12}$
wing weight [10]	10	$3.8 \cdot 10^{-1}$	$4.1 \cdot 10^{-1}$	$4.3 \cdot 10^{-3}$	$5.9 \cdot 10^{-2}$	$2.1 \cdot 10^{-10}$

significant of these occurs when the Lipschitz matrix is low-rank. If \mathbf{L} is rank- r and \mathcal{D} has intrinsic dimension m then \mathbf{LD} has intrinsic dimension r whose coordinates are given by the leading r right singular vectors of \mathbf{L} . In this case the growth of the covering number no longer depends exponentially on parameter space dimension m , but on the rank of \mathbf{L} . Even when \mathbf{L} is not exactly low rank, this same effect can slow the asymptotic growth in the covering number. When ϵ is sufficiently large as illustrated in Figure 6.1 there are dimensions of \mathbf{LD} that do not require more than one ϵ -ball to cover. This temporarily slows the growth of the covering number as shown in Figure 6.2. The second way the Lipschitz matrix reduces complexity emerges in the constants of the bounds (6.4) when \mathbf{L} is full rank. Both the lower and upper bounds depend on the volume of the transformed domain: $\text{vol}(LD)$ in the scalar Lipschitz case and $\text{vol}(\mathbf{LD})$ in the Lipschitz matrix case. These two volumes are proportional L^m and the determinant of \mathbf{L} :

$$(6.5) \quad \text{vol}(\mathbf{LD}) = |\det(\mathbf{L})| \cdot \text{vol}(\mathcal{D}), \quad \text{vol}(LD) = L^m \cdot \text{vol}(\mathcal{D}).$$

As illustrated in Table 6.1, the volume associated with the Lipschitz matrix is often orders of magnitude smaller than that associated with the scalar Lipschitz constant. This implies a substantial reduction in the number of function evaluations required to reach a specified accuracy when using the Lipschitz matrix as compared to the Lipschitz constant.

In the remainder of this section we connect the complexity of approximation, integration, and optimization of Lipschitz functions to the covering number.

6.1. Approximation Complexity. A key tool in establishing complexity results for Lipschitz functions is the *central approximation* \bar{f} : the mean of the lower and upper bounds of the uncertainty interval $\mathcal{U}(\mathbf{x}; \mathcal{L}(\mathcal{D}, \mathbf{L}), \{\hat{\mathbf{x}}_j, y_j\}_{j=1}^M)$ given in (4.5),

$$(6.6) \quad \mathcal{U}(\mathbf{x}) = \left[\max_{j=1, \dots, M} y_j - \|\mathbf{L}(\mathbf{x} - \hat{\mathbf{x}}_j)\|_2, \min_{j=1, \dots, M} y_j + \|\mathbf{L}(\mathbf{x} - \hat{\mathbf{x}}_j)\|_2 \right]$$

$$(6.7) \quad \bar{f}(\mathbf{x}) := \frac{1}{2} \left(\max_{j=1, \dots, M} y_j - \|\mathbf{L}(\mathbf{x} - \hat{\mathbf{x}}_j)\|_2 \right) + \frac{1}{2} \left(\min_{j=1, \dots, M} y_j + \|\mathbf{L}(\mathbf{x} - \hat{\mathbf{x}}_j)\|_2 \right).$$

The central approximation is the best worst-case approximation in the sup-norm.

LEMMA 6.1. *Given a Lipschitz matrix \mathbf{L} and data $\{\hat{\mathbf{x}}_j, y_j\}_{j=1}^M$ the central approximation \bar{f} (6.7) minimizes the worst case error over any other approximation*

$\tilde{f} \in \mathcal{L}(\mathcal{D}, \mathbf{L})$ where $\tilde{f}(\hat{\mathbf{x}}_j) = y_j$

$$(6.8) \quad \sup_{\substack{f \in \mathcal{L}(\mathcal{D}, \mathbf{L}) \\ f(\hat{\mathbf{x}}_j) = y_j \quad j=1, \dots, M}} |f(\mathbf{x}) - \bar{f}(\mathbf{x})| \leq \sup_{\substack{f \in \mathcal{L}(\mathcal{D}, \mathbf{L}) \\ f(\hat{\mathbf{x}}_j) = y_j \quad j=1, \dots, M}} |f(\mathbf{x}) - \tilde{f}(\mathbf{x})|.$$

This result allows us to show the worst case complexity of approximation of Lipschitz functions.

THEOREM 6.2. *The minimum number of samples required to construct an approximation $\tilde{f} \in \mathcal{L}(\mathcal{D}, \mathbf{L})$ of any Lipschitz function $f \in \mathcal{L}(\mathcal{D}, \mathbf{L})$ with maximum pointwise error ϵ , is the ϵ internal covering number of \mathbf{LD} , $N_\epsilon(\mathbf{LD})$.*

Proof. Consider the case where all observations of f are zero, i.e., $f(\hat{\mathbf{x}}_j) = 0$ for $j = 1, \dots, M$. From Lemma 6.1 the best approximation \tilde{f} is the central approximation \bar{f} whose worst-case error is, from (6.6),

$$(6.9) \quad \sup_{\substack{f \in \mathcal{L}(\mathcal{D}, \mathbf{L}) \\ f(\hat{\mathbf{x}}_j) = y_j \quad j=1, \dots, M}} |f(\mathbf{x}) - \bar{f}(\mathbf{x})| = \min_{j=1, \dots, M} \|\mathbf{L}(\mathbf{x} - \hat{\mathbf{x}}_j)\|_2.$$

The smallest number of samples such that this error is less than ϵ is $N_\epsilon(\mathbf{LD})$ by (6.3). Any other data $f(\hat{\mathbf{x}}_j)$ requires as many or fewer samples to obtain the same accuracy. \square

6.2. Optimization Complexity. The complexity of optimization follows a similar argument as that for approximation.

THEOREM 6.3. *The minimum number of samples to find the maximum of any Lipschitz function $f \in \mathcal{L}(\mathcal{D}, \mathbf{L})$ to within ϵ is $N_\epsilon(\mathbf{LD})$.*

Proof. First we provide an upper bound on the minimum number of samples. By Theorem 6.2, the central approximation constructed using $N_\epsilon(\mathbf{LD})$ samples is within ϵ of the Lipschitz function f ; i.e., $|f(\mathbf{x}) - \bar{f}(\mathbf{x})| \leq \epsilon$ for all $\mathbf{x} \in \mathcal{D}$. Hence at most $N_\epsilon(\mathbf{LD})$ samples are required to find the optimum of any $f \in \mathcal{L}(\mathcal{D}, \mathbf{L})$ within ϵ .

To show this bound is obtained, consider the function $f \in \mathcal{L}(\mathcal{D}, \mathbf{L})$ where $f(\mathbf{x}) \geq 0$ for all $\mathbf{x} \in \mathcal{D}$, $f(\mathbf{x}^*) = 2\epsilon$, and f has minimum integrand. Suppose we choose samples $\hat{\mathbf{x}}_j$ corresponding to an ϵ covering of \mathbf{LD} via (6.3); the location of \mathbf{x}^* can be chosen adversarially such that only the last sample has a value greater than ϵ , i.e., $f(\hat{\mathbf{x}}_j) < \epsilon$ for $j = 1, \dots, M-1$ and $f(\hat{\mathbf{x}}_M) \geq \epsilon$ where $M = N_\epsilon(\mathbf{LD})$. Hence $N_\epsilon(\mathbf{LD})$ samples are required to find the optimum of this function, obtaining the upper bound. \square

6.3. Integration Complexity. The quadrature rule with minimum worst case error is built using the same tools: the central approximation based on samples from a minimal ϵ -covering of \mathbf{LD} . This proof parallels the one-dimensional Lipschitz case presented by Traub and Werschulz [26, chap. 2].

THEOREM 6.4. *Let ϕ^* be the quadrature rule for functions $f \in \mathcal{L}(\mathcal{D}, \mathbf{L})$ resulting from integrating the central approximation \bar{f} constructed from $N_\epsilon(\mathbf{LD})$ samples $\hat{\mathbf{x}}_j^*$ solving (5.2)*

$$(6.10) \quad \int_{\mathcal{D}} f(\mathbf{x}) \, d\mathbf{x} \approx \phi^*(f) := \int_{\mathcal{D}} \bar{f}(\mathbf{x}) \, d\mathbf{x} \quad \text{where } \bar{f} \in \mathcal{L}(\mathcal{D}, \mathbf{L}) \text{ and } \bar{f}(\hat{\mathbf{x}}_j^*) = f(\hat{\mathbf{x}}_j^*)$$

and let ϕ be any other quadrature rule based on integrating an approximation \tilde{f} interpolating samples $\{\hat{\mathbf{x}}_j\}_{j=1}^{N_\epsilon(\mathbf{LD})}$

$$(6.11) \quad \int_{\mathcal{D}} f(\mathbf{x}) \, d\mathbf{x} \approx \phi(f) := \int_{\mathcal{D}} \tilde{f}(\mathbf{x}) \, d\mathbf{x} \quad \text{where } \tilde{f} \in \mathcal{L}(\mathcal{D}, \mathbf{L}) \text{ and } \tilde{f}(\hat{\mathbf{x}}_j) = f(\hat{\mathbf{x}}_j).$$

Then

$$(6.12) \quad \sup_{f \in \mathcal{L}(\mathcal{D}, \mathbf{L})} \left| \phi^*(f) - \int_{\mathcal{D}} f(\mathbf{x}) \, d\mathbf{x} \right| \leq \sup_{f \in \mathcal{L}(\mathcal{D}, \mathbf{L})} \left| \phi(f) - \int_{\mathcal{D}} f(\mathbf{x}) \, d\mathbf{x} \right|$$

and the error of ϕ^* is bounded above by $\epsilon \cdot \text{vol}(\mathcal{D})$.

Proof. First note that given set of points $\{\widehat{\mathbf{x}}_j\}_{j=1}^{N_\epsilon(\mathbf{L}\mathcal{D})}$, the central approximation has smallest worst case error by Lemma 6.1 and since $\bar{f}, \tilde{f} \in \mathcal{L}(\mathcal{D}, \mathbf{L})$ are Lipschitz continuous, the integrand of the central approximation has smaller worst case error than any other approximation interpolating the data. Then as using points $\widehat{\mathbf{x}}_j^*$ corresponding to the optimal covering of $\mathbf{L}\mathcal{D}$ via (6.3), the maximum pointwise error is ϵ . Integrating this over the domain yields the upper bound

$$(6.13) \quad \sup_{f \in \mathcal{L}(\mathcal{D}, \mathbf{L})} \left| \phi^*(f) - \int_{\mathcal{D}} f(\mathbf{x}) \, d\mathbf{x} \right| \leq \epsilon \cdot \text{vol}(\mathcal{D}). \quad \square$$

7. Discussion. Here we have generalized the scalar Lipschitz constant to the *Lipschitz matrix*. This Lipschitz matrix provides improved results over those for scalar Lipschitz functions: it yields more efficient designs for computer experiments, it decreases uncertainty, and it reduces the computational complexity of approximation, optimization, and integration. An appealing aspect of the Lipschitz matrix comes in its computation. Although the semidefinite program is expensive, it is a convex problem with a unique minimizer. Moreover, no restrictions are placed on how samples or gradients are chosen and either samples or gradients can be used. These are features not shared by any existing subspace based dimension reduction technique.

Acknowledgements. The authors would like to thank Akil Narayan for suggesting the counter example to maximum uncertainty designs in subsection 5.3 and Drew Kouri for pointing us to the randomized algorithms for Voronoi vertex sampling.

REFERENCES

- [1] M. S. ANDERSEN, J. DAHL, AND L. VANDENBERGHE, *CVXOPT: A Python package for convex optimization*, 2019, <http://cvxopt.org>.
- [2] F. AURENHAMMER AND R. KLEIN, *Voronoi diagrams*, in Handbook of Computational Geometry, J. Sack and J. Urrutia, eds., Elsevier Science, 2000, ch. 5.
- [3] C. B. BARBER, D. P. DOBKIN, AND H. T. HUHDANPAA, *The Quickhull algorithm for convex hulls*, ACM T. Math. Software, 22 (1996), pp. 469–483, <http://www.qhull.org>.
- [4] E. N. BEN-ARI AND D. M. STEINBERG, *Modeling data from computer experiments: An empirical comparison of kriging with MARS and projection pursuit regression*, Qual Eng, 19 (2007), pp. 327–338, <https://doi.org/10.1080/08982110701580930>.
- [5] S. BONNABEL AND R. SEPULCHRE, *Riemannian metric and geometric mean for positive semidefinite matrices of fixed rank*, SIAM J. Matrix Anal. A., 31 (2009), pp. 1055–1070, <https://doi.org/10.1137/080731347>.
- [6] P. G. CONSTANTINE, *Active Subspaces: Emerging Ideas for Dimension Reduction in Parameter Studies*, SIAM, Philadelphia, 2015.
- [7] P. G. CONSTANTINE, A. EFTEKHARI, J. HOKANSON, AND R. A. WARD, *A near-stationary subspace for ridge approximation*, Comput. Method. Appl. M., 326 (2017), pp. 402–421, <https://doi.org/10.1016/j.cma.2017.07.038>.
- [8] D. L. DONOHO, *High-dimensional data analysis: The curses and blessings of dimensionality*, in AMS Conference on Math Challenges of the 21st Century, 2000, <http://www-stat.stanford.edu/~donoho/Lectures/CBMS/Curses.pdf>.
- [9] V. V. FEDOROV, *Theory of Optimal Experiments*, Academic Press, New York, 1972.
- [10] A. I. J. FORRESTER, A. SÓBSTER, AND A. J. KEANE, *Engineering Design via Surrogate Modelling: A Practical Guide*, Wiley, 2008.

- [11] J. GOLINSKI, *Optimal synthesis problems solved by means of nonlinear programming and random methods*, J. Mechanisms, (1970), pp. 287–309, [https://doi.org/10.1016/0022-2569\(70\)90064-9](https://doi.org/10.1016/0022-2569(70)90064-9).
- [12] W. V. HARPER AND S. K. GUPTA, *Sensitivity/uncertainty analysis of a borehole scenario comparing latin hypercube sampling and deterministic sensitivity approaches*, tech. report, Battelle Memorial Institute, Oct. 1983.
- [13] J. M. HOKANSON AND P. G. CONSTANTINE, *Data-driven polynomial ridge approximation using variable projection*, SIAM J. Sci. Comput., 40 (2018), pp. A1566–A589, <https://doi.org/10.1137/17M1117690>.
- [14] M. E. JOHNSON, L. M. MOORE, AND D. YLVIKAKER, *Minimax and maximin distance designs*, J. Stat. Plan. Infer., 26 (1990), pp. 131–148, [https://doi.org/10.1016/0378-3758\(90\)90122-B](https://doi.org/10.1016/0378-3758(90)90122-B).
- [15] R. KENETT AND S. ZACKS, *Modern Industrial Statistics: Design and Control of Quality and Reliability*, Duxbury Press, Pacific Grove, CA.
- [16] J. A. LEE AND M. VERLEYSSEN, *Nonlinear Dimensionality Reduction*, Springer, 2007.
- [17] B. LI, *Sufficient Dimension Reduction: Methods and Applications with R*, CRC Press, 2018.
- [18] S. R. LINDEMANN AND P. CHENG, *Iteratively locating Voronoi vertices for dispersion estimation*, in Proceedings of the 2005 IEEE International Conference on Robotics and Automation, 2005, pp. 3862–3867, <https://doi.org/10.1109/ROBOT.2005.1570710>.
- [19] J. J. MORÉ AND S. M. WILD, *Estimating computational noise*, SIAM J. Sci. Comput., 33 (2011), pp. 1292–1314.
- [20] M. R. OSBORNE AND G. A. WATSON, *An algorithm for minimax approximation in the nonlinear case*, Comput. J., 12 (1969), pp. 63–68, <https://doi.org/10.1093/comjnl/12.1.63>.
- [21] C. E. RASMUSSEN AND C. K. I. WILLIAMS, *Gaussian Processes for Machine Learning*, MIT Press, 2006.
- [22] J. C. REGIER AND P. B. STARK, *Mini-minimax uncertainty quantification for emulators*, SIAM/ASA J. Uncert. Quant., 3 (2015), pp. 686–708, <https://doi.org/10.1137/130917909>.
- [23] J. SACKS, W. J. WELCH, T. J. MITCHELL, AND H. P. WYNN, *Design and analysis of computer experiments*, Stat. Sci., 4 (1989), pp. 409–435.
- [24] T. J. SANTER, B. J. WILLIAMS, AND W. I. NOTZ, *The Design and Analysis of Computer Experiments*, Springer, 2003.
- [25] S. SURJANOVIC AND D. BINGHAM, *Virtual library of simulation experiments: Test functions and datasets*, 2013, <http://www.sfu.ca/~ssurjano>.
- [26] J. F. TRAUB AND A. G. WERSCHULZ, *Complexity and Information*, Cambridge University Press, Cambridge, 1998.
- [27] P. WEI, Z. LU, AND J. SONG, *Variable importance analysis: A comprehensive review*, Reliab. Eng. Syst. Safe., (2015), pp. 399–432, <https://doi.org/10.1016/j.res.2015.05.018>.
- [28] Y. WU, *Lecture notes for ECE598YW: Information-theoretic methods for high-dimensional statistics*, <http://www.stat.yale.edu/~yw562/teaching/it-stats.pdf>.